Electronic Supplementary Material (ESI) for Physical Chemistry Chemical Physics.
This journal is © the Owner Societies 2022

Supporting information:

Understanding the evolution of the Raman spectra of molecularly p-doped poly(3-hexylthiophene-2,5-diyl): signatures of polarons and bipolarons

Ahmed E. Mansour,[1,2]†* Ana M. Valencia,[1,3]† Dominique Lungwitz,[1] Berthold Wegner,[1,2] Naoki Tanaka,[4]‡ Yoshiaki Shoji,[4] Takanori Fukushima,[4] Andreas Opitz,[1] Caterina Cocchi,[1,3] Norbert Koch[1,2]

1 Institut für Physik & IRIS Adlershof, Humboldt-Universität zu Berlin, 12489 Berlin, Germany

2 Helmholtz-Zentrum Berlin für Materialien und Energie GmbH, 12489 Berlin, Germany

3 Carl von Ossietzky Universität Oldenburg, Institute of Physics, 26129 Oldenburg, Germany

4 Laboratory for Chemistry and Life Science, Institute of Innovative Research, Tokyo Institute of Technology, Yokohama 226-8503, Japan

† These authors contributed equally to this work.

‡Present address: Department of Applied Chemistry, Graduate School of Engineering, Kyushu University, Fukuoka 819-0395, Japan

*amansour@physik.hu-berlin.de

Table S1: Raman active vibrational modes of neutral oligothiophene molecules (nT: n = 2, 3, 4, 5, 6). The modes are classified according to involved C-C bonds and the symmetric (sym) or asymmetric (asym) character of the oscillation. C atoms are shown in grey, H atoms in white, and S atoms in yellow.

nT	$[C_\alpha\text{-}C_\beta]_{sym}$	$[C_\alpha\text{-}C_\beta]_{asym}$
2T	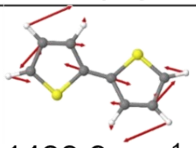 1439.9 cm^{-1}	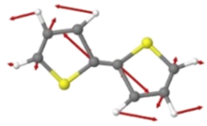 1537.0 cm^{-1}
3T	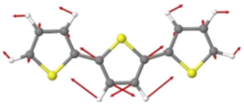 1454.5 cm^{-1}	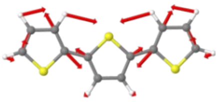 1513.9 cm^{-1}
4T	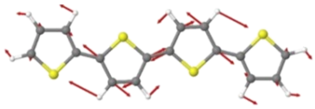 1448.8 cm^{-1}	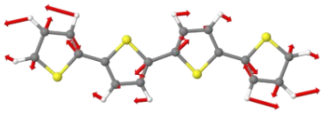 1500.2 cm^{-1}
5T	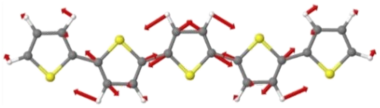 1441.7 cm^{-1}	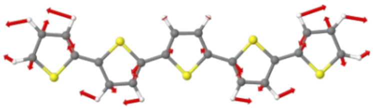 1493.6 cm^{-1}
6T	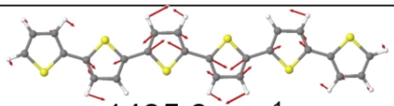 1435.9 cm^{-1}	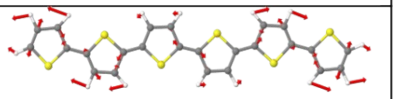 1488.26 cm^{-1}

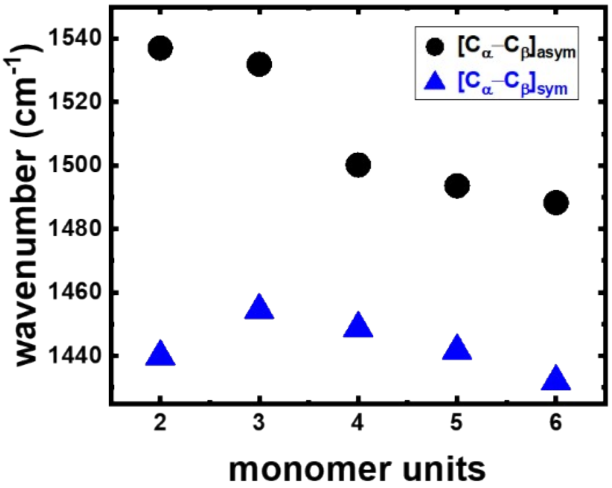

Figure S1: Calculated frequencies of the Raman active modes, $[C\alpha\text{-}C\beta]_{sym}$ and $[C\alpha\text{-}C\beta]_{asym}$, in neutral oligothiophene molecules as a function of the number of thiophene units.

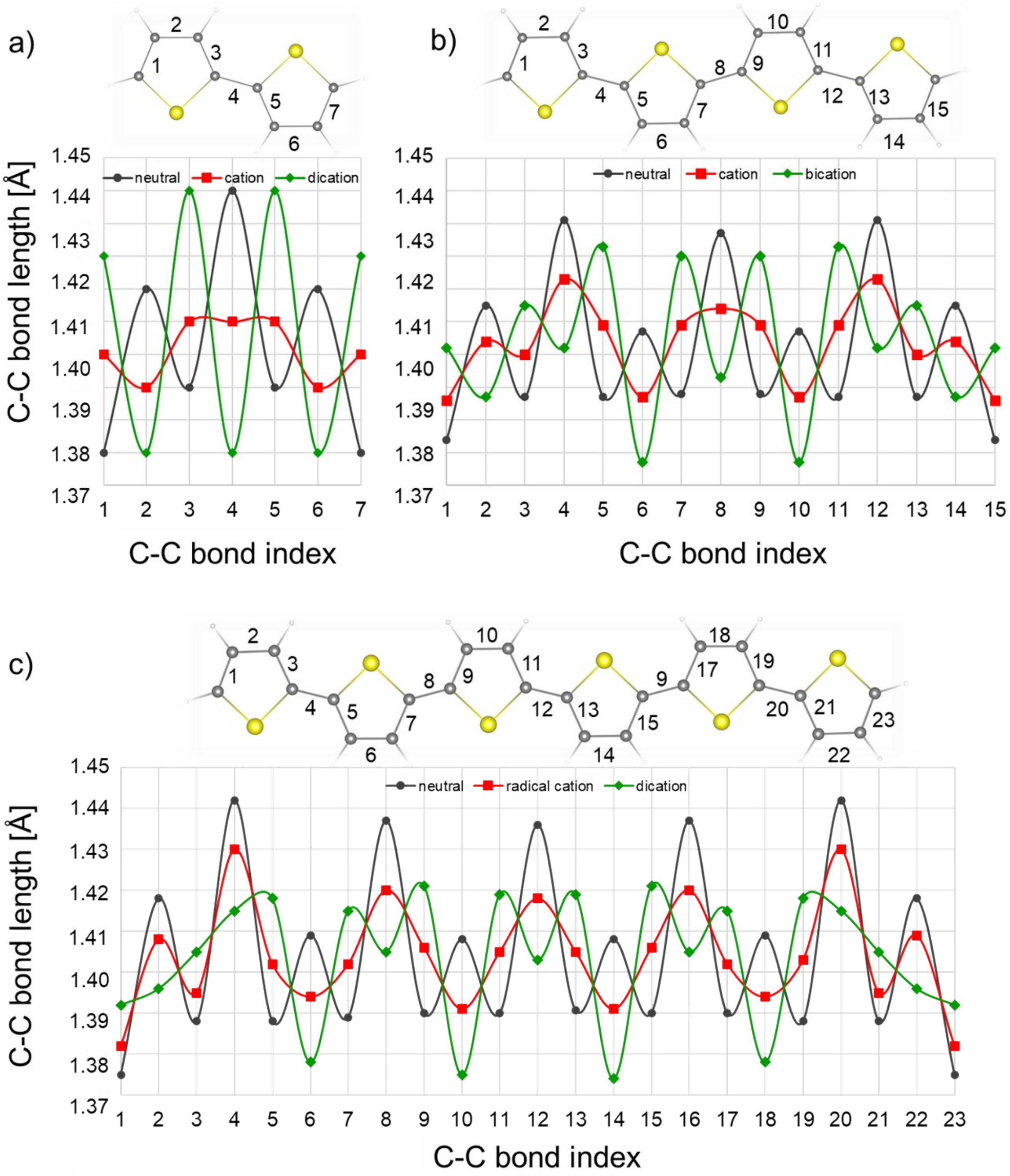

Figure S2: Representation of aromatic and quinoid structures. The C-C bond length variation in 2T, 4T, and 6T oligothiophenes in neutral, radical cation, and dication charged.

The C-C bond length analysis of 2T, 4T and 6T in their neutral, radical cation, and dication configurations shown in Figure S2, allows for the understanding of the effects of the charged defects in each structure. The charged oligomers have a different geometry than the neutral oligomer, which is manifested in the carbon-carbon bond length alternation (BLA). Considering as an example the shortest considered oligothiophene, 2T, when the (C-C) 1 and

(C-C) 3 bonds on one of the thiophene ring are shorter than the (C-C) 2 bond, the ring is considered aromatic. Conversely, when the (C-C) 1 and (C-C) 3 bonds on a thiophene ring are larger than the (C-C) 2 bond, the ring is considered quinoid[1,2]. The distinction between an aromatic structure and a quinoid one makes it possible to determine the location and extent of the defect. Following the data reported for each oligomer there is a clear pattern when connecting three C-C bonds: the ʌ-shape corresponds to an aromatic BLA pattern in the rings, while the V-shape corresponds to the quinoid rings of a charged oligomer. The bonds between the rings are shortened and take on a double bond character in the quinoid structure, which therefore also points to the location of the charge. This behavior is a manifestation of the formation of a charged polymer chain segments.

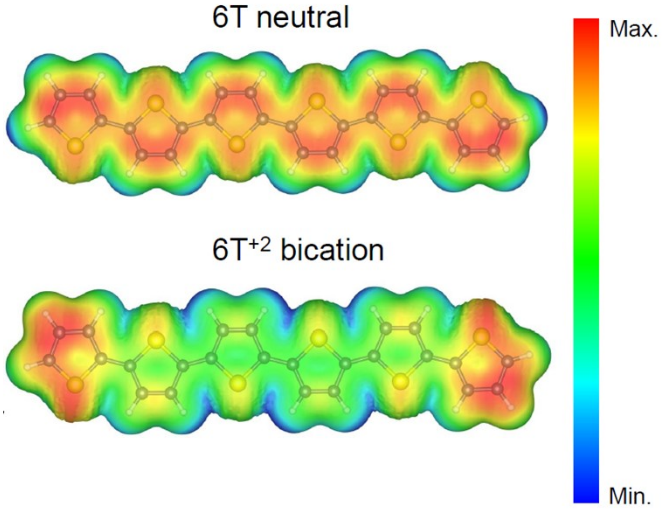

Figure S3: Calculated electrostatic potential energy of an isosurface with the total electron density of 0.006 e/Å^3 in 6T neutral and 6T^{+2}dication oligomer. The red and blue stand for negative and positive potential regions, respectively.

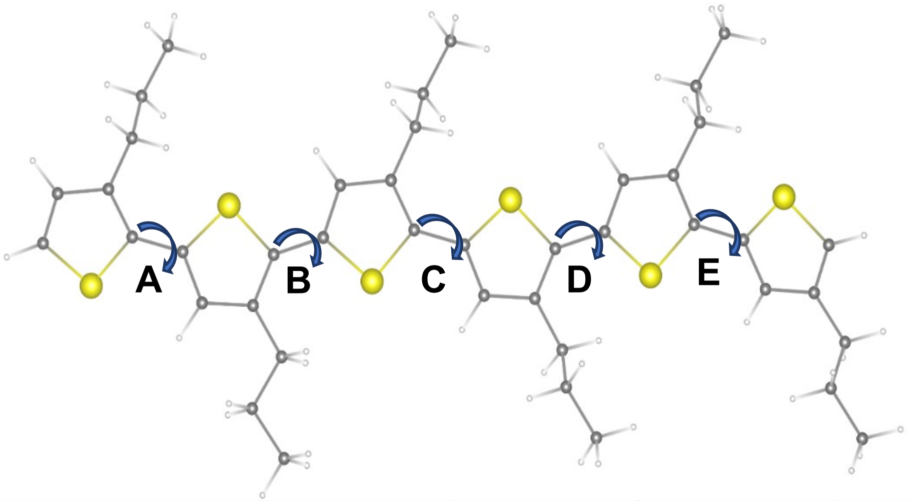

Dihedral angle [°]	**A**	**B**	**C**	**D**	**E**
neutral	31.1	0.7	26.6	28.3	33.8
radical cation	7.5	0.2	3.7	6.8	13.6
dication	0.1	0.1	0.1	0.1	0.1

Figure S4: (Top) Representation of 6T with C_3H_7 groups attached and the dihedral angle variation in neutral, radical cation, and dication oligothiophenes. (Bottom) Dihedral angles between adjacent rings visualized on the top panels.

In a vacuum, the alkyl chain gives 6T great structural freedom, which affects the planarization of the π-conjugated oligomer. In our analysis, summarized in Figure S3, we focus on the dihedral angle as well as on the bond length of the three 6T, 6T$^{\bullet+}$, and 6T^{2+} oligomers. In neutral 6T, the value of the torsional angle ranges from 31.1° to 33.8° from one edge to the other. Once the 6T is charged, the structure exhibits a planarization indicated by dihedral angles going from 13.6° at one edge to 7.5° at the opposite edges, although in the middle of the structure the angle variation decreases considerably already in 6T$^{\bullet+}$, while planarity is obtained in 6T^{2+}. Our results are in agreement with previous theoretical results.[3,4] The analysis of the bond length in each structures follow the same trend obtained on the 6T oligomers without alkyl chain reported in Figure S2.

Assignment of the calculated vibrational modes:

Vibrational Raman spectra are computed in the harmonic approximation, we calculate the harmonic Raman intensity $I_H(\omega)$ which is proportional to the Raman scattering cross section[5,6] of a given normal mode p by,

$$I_H(\omega) = I_H^{\perp} + I_H^{\parallel} \propto \frac{1}{\omega(1 - \exp(\beta\omega\hbar))} \frac{1}{30}\left(10G_p^{(0)} + 7G_p^{(2)}\right),$$

$$G_p^{(0)} = \frac{1}{3}\left[(\alpha_{xx}^{'})_p + (\alpha_{yy}^{'})_p + (\alpha_{zz}^{'})_p\right]^2,$$

$$G_p^{(2)} = \frac{1}{2}\left[2(\alpha_{xy}^{'})_p^2 + 2(\alpha_{xz}^{'})_p^2 + 2(\alpha_{yz}^{'})_p^2\right] + \frac{1}{3}\left\{\left[(\alpha_{xx}^{'})_p - (\alpha_{yy}^{'})_p\right]^2 + \left[(\alpha_{xx}^{'})_p - (\alpha_{zz}^{'})_p\right]^2 + \left[(\alpha_{yy}^{'})_p - (\alpha_{zz}^{'})_p\right]^2\right\},$$

Where $I_H^{\perp}$ and $I_H^{\parallel}$ are the depolarized and polarized Raman intensities, $\beta = 1/k_BT$, and $(\alpha_{ij}^{'})_p = (\partial\alpha_{ij}/\partial Q_p)_0$ is the derivative of the ij component of the polarizability with respect to the displacement of normal mode Q_p. These derivatives are computed by finite differences, where we evaluate the polarizability tensor from density functional perturbation theory (DFPT)[7] at 6N (with N being the number of atoms per molecule) nuclear displacements in the molecule around the equilibrium position.

The assignment of the C_α-C_β vibrations is not straightforward, since the characteristic peaks observed in the measured Raman spectrum originate from collective skeletal and symmetric stretching or asymmetric deformations in the thiophene units extending over a large portion of the backbone. In symmetric vibrations, double-bonded carbons across several thiophene units are stretching simultaneously in the same direction (in-phase stretching mode), while in asymmetric vibrations, a pair of double-bonded carbons are stretching while another such pair is contracting. The asymmetric stretching modes are Raman active when adjacent thiophene units are in-phase (in-phase deformation mode).[8] Since assignment based on visual inspection is hardly conclusive, we relied first on the calculated Raman activity values for each vibration (shown as percentages of the largest activity in Table S2). Afterwards, visual inspection of the vibrations was used to confirm that it is the expected vibration mode. According to this procedure, the assigned vibrations for 6T along with their respective assignments in the polaron and bipolaron cases are shown in Figures S5.

Table S2: Calculated vibrational frequency and Raman activities of 6T in the neutral, charged (+1) and double charged (+2) configurations. Highlighted vibrations are the ones assigned to the vibrational modes as follows: green: C_β-C_β “ν_2”, blue: $[C_\alpha$-$C_\beta]_{sym}$ “ν_1”, orange: $[C_\alpha$-$C_\beta]_{asym}$ “ω_3”, and yellow: out-of-phase deformation of the rings “ω_4”. The vibrational modes written in red are the new Raman modes that appear in the charged states of P3HT as discussed in the main text.

Neutral			**+1**			**+2**		
#	**energy (cm^{-1})**	**activity (%)**	**#**	**energy (cm^{-1})**	**activity (%)**	**#**	**energy (cm^{-1})**	**activity (%)**
103	1323.80	0%	103	1330.63	16%	103	1332.65	2%
104	1347.59	0%	104	1354.13	23%	104	1352.41	43%
105	1365.40	0%	105	1378.17	0%	105	1377.57	0%
106	1377.85	2%	106	1406.74	100%	106	1408.90	19%
107	1434.86	0%	107	1415.88	0%	107	1414.86	0%
108	1432.04	100%	108	1424.36	34%	108	1428.45	100%
109	1435.86	87%	109	1428.22	17%	109	1431.53	2%
110	1448.28	0%	110	1440.01	0%	110	1439.99	52%
111	1454.57	6%	111	1443.39	0%	111	1463.66	0%
112	1457.25	0%	112	1460.48	0%	112	1470.77	0%
113	1473.61	0%	113	1467.66	14%	113	1482.86	0%
114	1488.26	17%	114	1471.17	0%	114	1486.59	1%
115	1507.68	0%	115	1487.54	5%	115	1498.23	0%
116	1527.85	1%	116	1506.75	4%	116	1499.65	0%
117	1542.88	0%	117	1520.00	0%	117	1507.37	0%
118	1550.46	0%	118	1527.34	10%	118	1516.10	1%

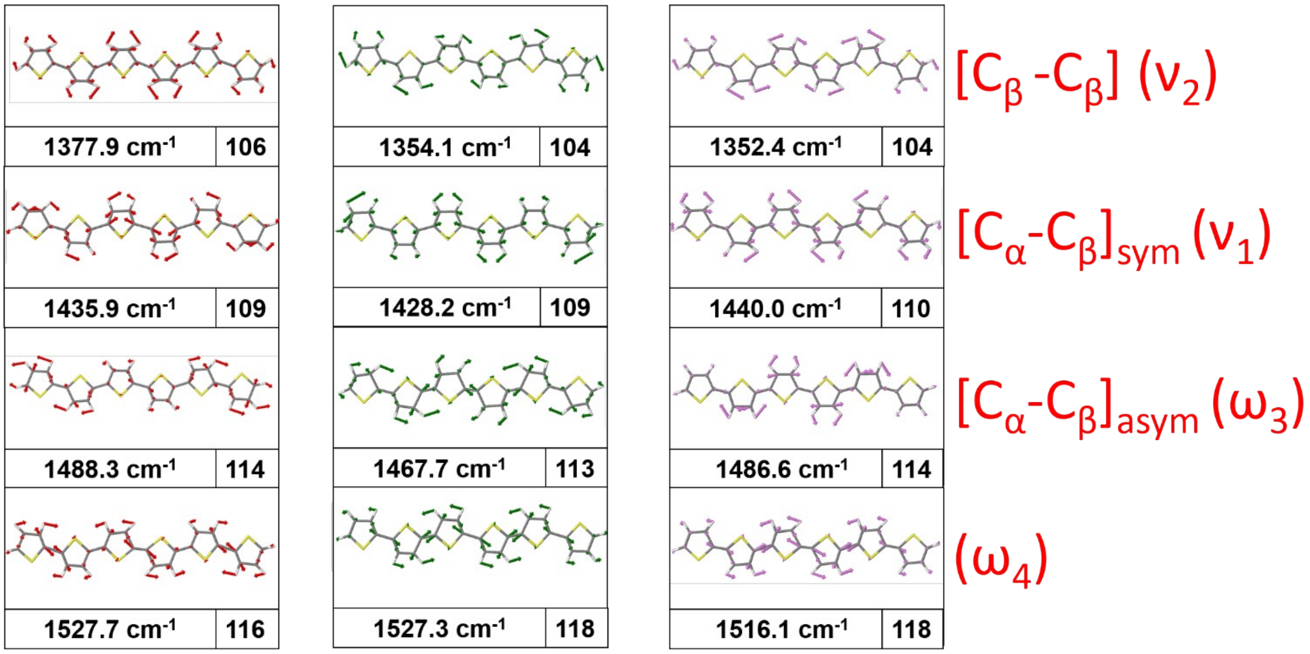

Figure S5: The calculated atomic displacement and their respective frequency and number of vibrational modes as shown in Table S2. The labels of vibrational modes between the parenthesis are as defined in Brambilla et al.[8] and provided for direct comparison with literature.

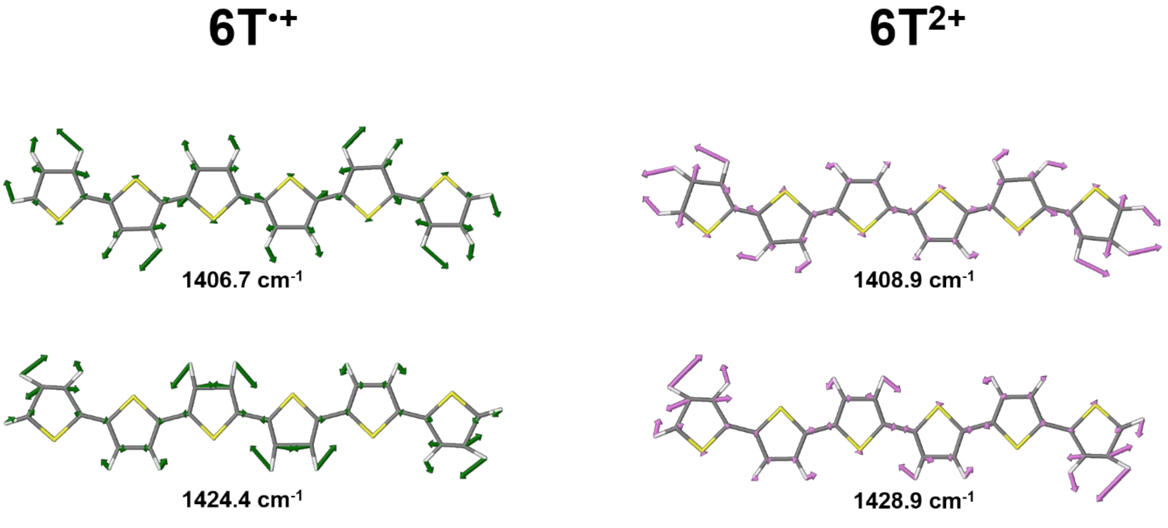

Figure S6: Calculated atomic displacements and respective frequencies of the vibrational modes related to the quinoid structure in charged 6T. These vibrations are labelled in red in Table S2.

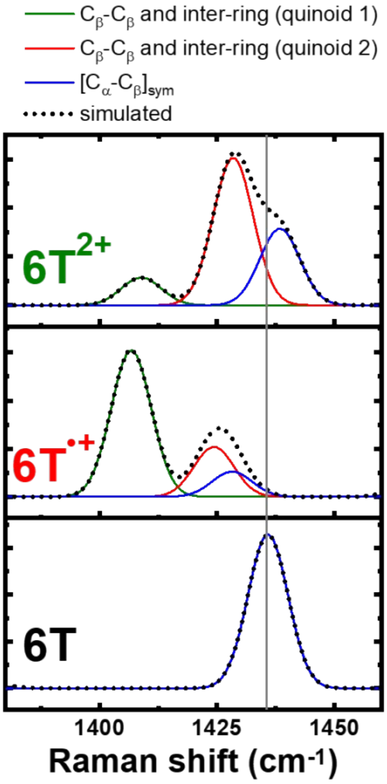

Figure S7: Raman spectra calculated around the $[C_\alpha$-$C_\beta]_{sym}$ peak for sexithiophene oligomer neutral state (6T), in the radical cation ($6T^{\bullet+}$), and in the dication ($6T^{2+}$). The peaks related to the vibrations in the quinoid structure (in Figure S6) are included. A Gaussian broadening of 10 cm^{-1} is applied to all spectra. The vertical line traces the $[C_\alpha$-$C_\beta]_{sym}$ peak.

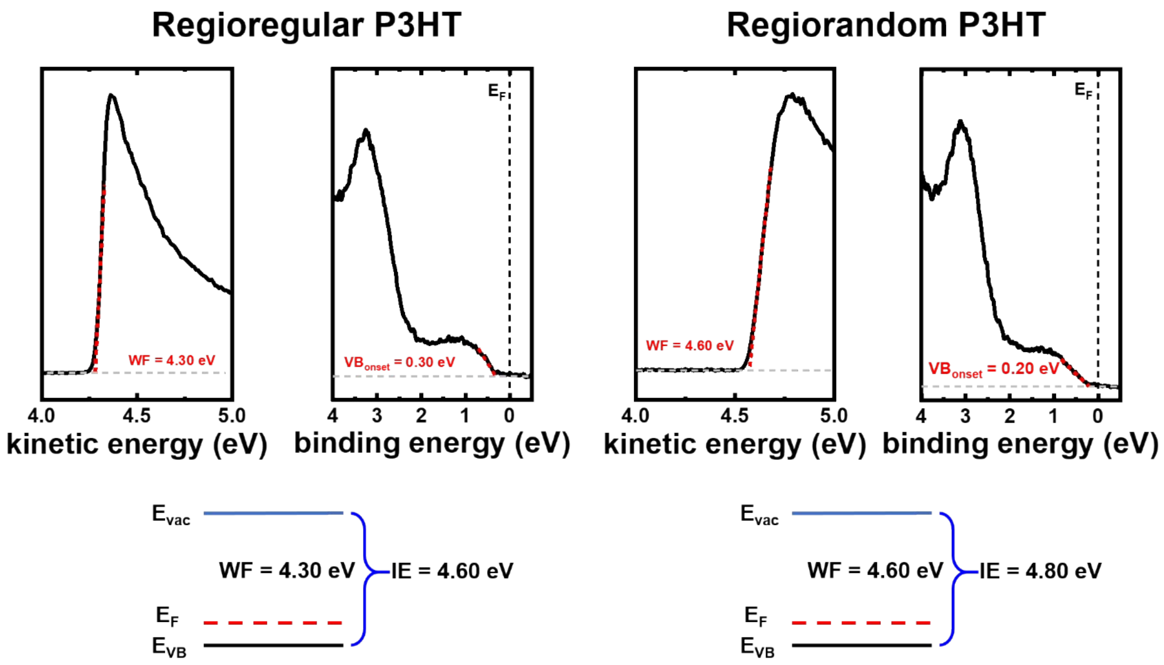

Figure S8: UPS measurements on rr-P3HT and rra-P3HT, showing the secondary electron cut-off (SECO) measured with bias of -10 V, and the valence band spectra close to the Fermi level. The Ionization energy (IE) in the schematic below the spectra is obtained by adding the work function (WF) of the sample represented by the onset of the SECO on the kinetic energy scale, and the valence band onset (VB_{onset}).

(1) Geskin, V. M.; Brédas, J. L. Polaron Pair versus Bipolaron on Oligothiophene Chains: A Theoretical Study of the Singlet and Triplet States. *ChemPhysChem* **2003**, *4* (5), 498–505. https://doi.org/10.1002/cphc.200200446.

(2) Ziaei, V.; Bredow, T. Simple Many-Body Based Screening Mixing Ansatz for Improvement of GW/Bethe-Salpeter Equation Excitation Energies of Molecular Systems. *Phys. Rev. B* **2017**, *96* (19), 195115. https://doi.org/10.1103/PhysRevB.96.195115.

(3) Nightingale, J.; Wade, J.; Moia, D.; Nelson, J.; Kim, J. Impact of Molecular Order on Polaron Formation in Conjugated Polymers. *J. Phys. Chem. C* **2018**, *122* (51), 29129–29140. https://doi.org/10.1021/acs.jpcc.8b09706.

(4) Krumland, J.; Valencia, A. M.; Cocchi, C. Exploring Organic Semiconductors in Solution: The Effects of Solvation, Alkylization, and Doping. *Phys. Chem. Chem. Phys.* **2021**, *23* (8), 4841–4855. https://doi.org/10.1039/D0CP06085B.

(5) Murphy, W. F.; Brooker, M. H.; Nielsen, O. F.; Praestgaard, E.; Bertie, J. E. Further Assessment of Reduction Procedures for Raman Spectra. *J. Raman Spectrosc.* **1989**, *20* (10), 695–699. https://doi.org/10.1002/jrs.1250201010.

(6) Prosandeev, S. A.; Waghmare, U.; Levin, I.; Maslar, J. First-Order Raman Spectra of AB1 2′B1 2″O3 Double Perovskites. *Phys. Rev. B - Condens. Matter Mater. Phys.* **2005**, *71* (21), 214307. https://doi.org/10.1103/PhysRevB.71.214307.

(7) Shang, H.; Raimbault, N.; Rinke, P.; Scheffler, M.; Rossi, M.; Carbogno, C. All-Electron, Real-Space Perturbation Theory for Homogeneous Electric Fields: Theory, Implementation, and Application within DFT. *New J. Phys.* **2018**, *20* (7), 073040. https://doi.org/10.1088/1367-2630/aace6d.

(8) Brambilla, L.; Capel Ferrón, C.; Tommasini, M.; Hong, K.; López Navarrete, J. T.; Hernández, V.; Zerbi, G. Infrared and Multi-Wavelength Raman Spectroscopy of Regio-Regular P3HT and Its Deutero Derivatives. *J. Raman Spectrosc.* **2018**, *49* (3), 569–580. https://doi.org/10.1002/jrs.5301.